THERMO-HYDRO-MECHANICAL COUPLING IN CLAY BARRIERS

F. Collin, X.L. Li, & R. Charlier, J.P.Radu
Département MSM, Université de Liège, Belgium, and ALERT GEOMATERIALS

ABSTRACT: A complete thermo-hydro-mechanical model is presented to treat the complex coupling problems in the clay barrier. The formulation related to the heat transfer, moisture transfer (liquid water and water vapour), air transfer in a deformable unsaturated soil is given. The formulation of the Alonso-Gens's mechanical model for unsaturated soil is also incorporated. Finally, a small scale wetting – heating test on compacted bentonite is performed as a validation test. The numerical results are compared with respect to the experimental measurements.

1.INTRODUCTION

Some nuclear waste disposal concepts are based on the waste storage in deep clay geological layers. The nuclear canister are surrounded by highly compacted clay, which undergoes a very high suction (up to 100 MPa or more) and this suction modifies the hydro-mechanical behaviour. Moreover the confinement barrier is subjected to high temperature (over 70°C and sometimes over 100°C). A good design of a clay barrier should take all these phenomena into account. For this purpose, constitutive laws have been developed. They are coupling the water flow, the heat flow and the soil mechanic. They have been implemented in a finite element code, which allows analysing non-homogenous transient problems.

The mechanical behaviour of a partly saturated soil is depending of the stress level and of the suction. A refined model has been proposed ten years ago by Alonso and Gens. The water flow in unsaturated media is a non-linear problem. Moreover high temperature induces the production of water vapour (which depends also on the suction level). Its modelling is based on the Philip's and de Vries's contribution.

The developed finite elements are based on the following degrees of freedom: soil skeleton displacements, temperature, liquid water pressure, and gas (dry air + vapour) pressure. The elements have a monolithically form, and all coupling terms are taken in the Newton-Raphson stiffness matrix into account, allowing a good convergence rate for most treated problems.

A validation of the constitutive laws and of the finite element code is obtained thanks to a comparison with other code results and with some experimental results.

2. DIFFUSION MODEL

In the clay barriers, the unsaturated conditions and the thermal variations create several coupling effects that influenced the design of each component of the barriers. Moreover high temperature in unsaturated conditions induces the production of water vapour. Thus, the liquid water and the dissolved air compound the liquid phase. The gas phase is a mixture of dry air and water vapour.

The variables chosen for the description of the flow problem are the liquid water pressure, the gas pressure and the temperature.

2.1 Water species

The mass conservation equation is written for the mass of liquid water and water vapour. There will be significant effects of vapour flows only if the liquid and the vapour flows have a same order of magnitude.

Clay presents a very low permeability and very slow liquid water motions. So the effect of water vapour transport in this type of soil may not be neglected.

2.1.1 Conservation of the water mass

The equation includes the variation of the water storage and the divergence of water flows, including the liquid and vapour effects:

$$\frac{\partial \rho_w n S_{r,w}}{\partial t} + div(\rho_w \underline{f}_w) + \frac{\partial \rho_v n S_{r,g}}{\partial t} + div(\rho_v \underline{f}_v + \rho_v \underline{f}_g) = 0 \quad (2.1)$$

where ρ_w is the liquid water density; n is the medium porosity; $S_{r,w}$ is water saturation degree in volume; $\underline{f}_\alpha$ is the macroscopic velocity of the component α; ρ_v is the water vapour density; $S_{r,g}$ is the gas saturation degree in volume and t is the time.

Vapour flows thanks to the vapour diffusion in the medium and to the gas convection.

2.1.2 Motion of liquid water

Liquid water velocity is given by the generalised Darcy's law for multiphase porous medium:

$$\underline{f}_w = -\frac{k_{\text{int}} k_{r,w}}{\mu_w}\left[\underline{\nabla} p_w + g\rho_w \underline{\nabla} y\right] \quad (2.2)$$

where p_w is the liquid water pressure; y is the vertical, upwards directed co-ordinate; g is the gravity acceleration; μ_w id the dynamic viscosity of the liquid water; k_{int} is the intrinsic permeability of the medium and $k_{r,w}$ is the water relative permeability.

The water permeability varies with respect to the saturation degree in unsaturated conditions.

2.1.3 Coupling effects

The liquid water properties (i.e. density and viscosity) depend on temperature. This induces a coupling between the liquid water flow and the thermal flow: some convective water flows can be created due to the temperature distribution. Another coupling effect is due to the permeability which depends on suction (i.e the difference between the gas and water pressure). The suction field will influence the water flows.

2.1.4 Diffusion of water vapour

The water vapour flow expression is based on a Philip's and de Vries's model (Philip & de Vries 1957):

$$\underline{f}_v = -[D_{atm} \nu_v \tau_v n S_{r,g} / \rho_v] \underline{\nabla} \rho_v \quad (2.3)$$

where D_{atm} is the diffusion coefficient; ν_v is the 'mass flow' factor and τ_v is the tortuosity.

This relation is very similar to a diffusion Fick's law and shows that the vapour diffusion is due to a gradient of vapour density.

The water vapour density ρ_v is given by thermodynamic relations (Edlefsen & Anderson 1943):

$$\rho_v = \rho_0 h \quad (2.4)$$

where ρ_0 is the saturated water vapour density and h is the relative humidity.

The relative humidity h is given by the Kelvin-Laplace's law:

$$h = \exp\left(\frac{p_w - p_g}{\rho_w R_v T}\right) \quad (2.5)$$

where R_v is the gas constant of water vapour.

The relative humidity allows taking into account adsorption phenomena and capillary effect in the soil.

The vapour is considered as a perfect gas and the vapour pressure is given by the perfect gas law:

$$p_v = \rho_v R_v T \quad (2.6)$$

The gradient of the water vapour density can now be developed in order to compute the vapour flow:

$$\underline{\nabla} \rho_v = \frac{\rho_0 g h}{R_v T} \underline{\nabla} \frac{p_w - p_g}{\rho_w g} + \left[h \frac{\partial \rho_0}{\partial T} - \frac{\rho_0 (p_w - p_g) h}{\rho_w R_v T^2} \right] \underline{\nabla} T \quad (2.7)$$

The water vapour density gradient can be separated into two contributions: an isothermal one related to a suction gradient and a thermal one due to a temperature gradient.

2.1.5 Coupling effect

As shown above, the vapour properties and flows depend essentially on the temperature and on the gas pressure fields. This model can reproduce the vapour transport from the points at high temperature (where the water vapour is produced) to the points at lower temperature (where the water vapour condenses).

2.2 Dry air species

Dry air is a part of a gas mixture: dry air and water vapour compose the gas phase. But there is also dissolved air in the water that has to be taken into account. The dry air pressure is not a basic variable: this pressure will be computed up to the gas and the vapour pressure.

Dalton's law is assumed: the pressure of the gas mixture is equal to the sum of the partial pressures which each gas would exert if it filled alone all the volume considered.

2.2.1 Conservation of the dry air mass

The equation of mass conservation includes the contributions of the dry air phase and of the dissolved air in water:

$$\frac{\partial \rho_a n S_{r,g}}{\partial t} + div(\rho_a \underline{f}_g) + \frac{\partial H \rho_a n S_{r,w}}{\partial t} + div(H \rho_a \underline{f}_w) = 0 \quad (2.8)$$

where ρ_a is the dry air density and H the Henry's coefficient.

The Henry's coefficient H allows to determine the dissolved air in the liquid water. The dissolved air mass is supposed to be sufficiently low in order to consider that the water properties do not be influenced. The dry air flow is due to the flow of the gas mixture which has to be defined.

2.2.2 Motion of gas

The gas velocity is given by the generalised Darcy's law for multiphase medium:

$$\underline{f}_g = -\frac{k_{\text{int}} k_{r,g}}{\mu_g}\left[\underline{\nabla} p_g + g \rho_g \underline{\nabla} y\right] \quad (2.9)$$

where μ_g is the gas dynamic viscosity; $k_{r,g}$ is the gas relative permeability and ρ_g is the gas density.

The gas permeability is adapted in order to reproduce its variation in non-saturated conditions.

2.3 Heat diffusion

2.3.1 Heat conservation equation

$$\frac{\partial \phi}{\partial t} + div(\underline{q}) - Q = 0 \quad (2.10)$$

where ϕ is the enthalpy of the medium; $\underline{q}$ is the heat flow and Q is a volume heat source.

2.3.2 Heat storage: Enthalpy

The enthalpy of the system is given by the sum of the enthalpy of each component:

$$\begin{aligned}\phi = {} & n S_{r,w} \rho_w c_{p,w} (T - T_0) + n S_{r,g} \rho_a c_{p,a} (T - T_0) \\ & + (1-n) \rho_s c_{p,s} (T - T_0) + n S_{r,g} \rho_v c_{p,v} (T - T_0) \\ & + n S_{r,g} \rho_v L\end{aligned} \quad (2.11)$$

where $c_{p,\alpha}$ is the specific heat of the component α. The last enthalpy term corresponds to the stored heat during the water vaporisation.

2.3.3 Heat transport

Three heat transport terms are taken into account: they represent the conductive effect, the convective one and the vaporisation one.

$$\begin{aligned}\underline{q} = {} & -\Gamma \underline{\nabla} T + \phi_w \frac{\underline{f}_w}{n S_{r,w}} + \phi_a \frac{\underline{f}_g}{n S_{r,g}} + \phi_v \frac{\underline{f}_g}{n S_{r,g}} \\ & + c_{pv} \rho_v \underline{f}_v (T - T_0) + \left(\rho_v \underline{f}_v + \rho_v \underline{f}_g\right) L\end{aligned} \quad (2.12)$$

where Γ is the conductivity if the medium.

The solid convection is also explicitly modelled by some authors. Our model is taking the large strains and large rotations of the sample into account, thanks to a Lagrangian actualised formulation. Therefore the equilibrium and balance equation, as well as the water, air, and heat flow are expressed in the current configuration. This implies that the solid convection effect is implicitly taken into account.

2.3.4. Coupling effect

The principal coupling effect results from the convection: a quantity of heat is transported by water, vapour and air flow.

3 MECHANICAL BEHAVIOUR MODELLING

The suction has a strong influence on the mechanical properties of soil: the hardness and the shear strength of soil increase with suction; the swelling or collapse can be induced, even some irreversible deformations can take place… So, the mechanical behaviour modelling should be able to take these suction effects into account.

The applications of the concept of *effective stress* to the mechanical behaviour modelling of an unsaturated soil have some limitations. The use of the *independent stresses state variables* to model the

mechanical behaviour of unsaturated soils seems to be more and more convincible (Fredlund & Morgenstern 1977). That is:

$$\begin{aligned} &\text{net stresses tensor}: \sigma^*_{ij} = \sigma_{ij} - p_g \delta_{ij} \\ &\text{the suction}: \qquad s = p_g - p_w \end{aligned} \tag{3.1}$$

Alonso et al (Alonso et al. 1990) has proposed a mechanical model, which is written in the framework of the *independent stresses state variables*. It is based on the well-known CamClay model. In our finite element code *LAGAMINE*, the plastic yield surfaces are written in a three-dimensional stress space: $I^*_\sigma - II^*_{\hat{\sigma}} - s$ where I^*_σ is the first net stress invariant and $II^*_{\hat{\sigma}}$ refers to the second net deviatoric stress invariant.

The yield surface in the $I^*_\sigma - II^*_{\hat{\sigma}}$ space named F_1 at a given value of suction is written as:

$$F_1 = \left(I^{*2}_\sigma + (I_0 - P_s) I^*_\sigma - I_0 P_s\right)\bar{r}^2 + II^{*2}_{\hat{\sigma}} \tag{3.2}$$

where $\bar{r}$ represents the failure states of soil and depend on the Lode's angle. P_s characterise the resistance of soil on extension and varies with the suction. I_0 refers to the pre-consolidation of soil and is a function of the suction (Fig. 3.2):

$$I_0 = p_c \left(\frac{I^*_0}{p_c}\right)^{\frac{\lambda(o)-\kappa}{\lambda(s)-\kappa}} \tag{3.3}$$

where I^*_0 represents the pre-consolidation pressure of soil in saturated condition. p_c is a reference pressure. $\lambda(s)$ refers to the plastic slope of the compressibility curve against the net mean stress, it varies with the suction followed by:

$$\lambda(s) = \lambda(0)\left[(1-r)\exp(-\beta s) + r\right] \tag{3.4}$$

$\lambda(0)$ is the plastic slope for the saturated condition. κ, the elastic slope of the compressibility curve against the net mean stress, may also be function of the suction. r and β are parameters.

The irreversible deformation upon drying can be modelled with the help of another yield surface (*SI*) in the $I^*_\sigma - s$ plan, named F_2 (Fig. 3.1):

$$F_2 = s - s_0 \tag{3.5}$$

where s_0 is a yield suction value which represents the maximum value of suction submitted by the soil.

The preconsolidation pressure curve in the $I^*_\sigma - s$ plan (equation 3.3) defines another part of the yield surface called LC (Loading Collapse) which serves for modelling the collapse behaviour under wetting.

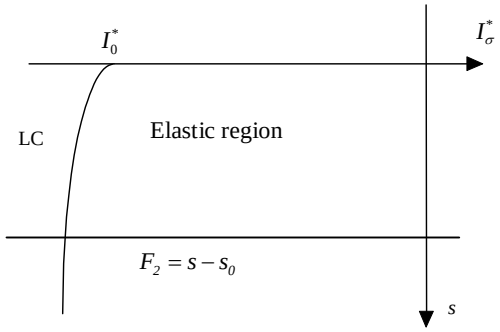

Figure 3.1. Yield surface in the plan $I^*_\sigma - s$

The model responses include principally three parts.

The strains induced by stress variations (mechanical solicitation) are given by:

$$\begin{aligned} &\dot{\sigma}^e_{ij} = C^e_{ijkl}\dot{\varepsilon}^e_{kl} \ \text{(elastic deformations)} \\ &\dot{\varepsilon}^p_{ij} = \dot{\lambda}\frac{\partial G}{\partial \sigma_{ij}} \ \text{(plastic deformations)} \end{aligned} \tag{3.6}$$

where C^e_{ijkl} is the Hook's tensor, $\dot{\sigma}^e_{ij}$ is the elastic net stress tensor, G is the plastic potential surface, and $\dot{\lambda}$ is obtained by the consistency condition.

The deformations induced by the suction evolution (hydric path) are:

$$\begin{aligned} &\dot{\varepsilon}^e_{kl-s} = \frac{\kappa_s}{3(1+e)(s+P_{at})}\dot{s}\delta_{kl} \ \ (\text{if } s < s_0) \\ &\dot{\varepsilon}^p_{kl-s} = \frac{\lambda_s - \kappa_s}{3(1+e)(s+P_{at})}\dot{s}\delta_{kl} \ \ (\text{if } s \geq s_0) \end{aligned} \tag{3.7}$$

where λ_s and κ_s are the stiffness parameters for changes in suction and P_{at} is the atmospheric pressure. It should be noted that λ_s and κ_s could vary with the stress level.

The elastic thermal dilatation of soil is introduced in the model by:

$$\dot{\varepsilon}^e_{kl-T} = \alpha \dot{T}\delta_{kl} \tag{3.8}$$

where α is the dilatation coefficient of soil.

The yield surface evolution is controlled by the total plastic volumetric strain ε^p_v developed in the soil via two state variables I^*_0 and s_0.

This version of model can reproduce the swelling and collapse behaviours but has some limitations for

highly expansive materials: the plastic swelling deformation can't be taken into account.

4. VALIDATION TESTS

In the framework of a European Community research project entitled *Calculation and testing of behaviour of unsaturated clay (Catsius clay)*, to investigate both temperature and artificial hydration effects on the deformation and moisture transfer in the soil, a small-scale wetting-heating test has been performed on highly compacted bentonite. The test has been performed inside a thermohydraulic cell, which is schematised in figure 4.1. The sample has been heated by means of the central heater and hydrated through the ports that are connected to the porous plate. During the test, the temperatures at different points, the volume of water flow and the swelling pressures generated in the sample have been measured. The outer cell surface has been in contact with ambient air. The experience has elapsed during 2401.6 hours.

A finite element simulation is realised with the help of the developed finite elements with five-freedom degrees. The heating is modelled by imposing the temperature on the nodes of the sample in contact with the heater. The hydration procedure is modelled by increasing the water pressure on the nodes of porous plate. The convection transfer between the steel case and the ambient atmosphere is modelled thanks to the frontier thermal elements.

The steel case is supposed to be impermeable to the water flow. Both steel case and porous plate deformations are neglected. The system is initially at the ambient temperature (293 °K). The gas pressure remains fixed to the atmospheric pressure (100 kPa). The initial saturation of soil is *49%* which gives an initial suction s =78.6 MPa according to the water retention curve.

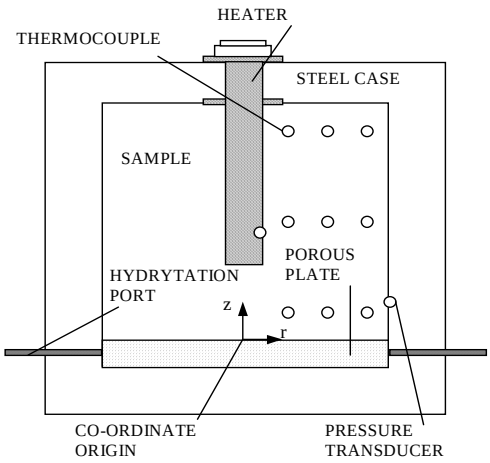

Fig. 4.1 Configuration of the thermohydraulic cell

4.1 Hydraulic and thermal properties

An equation describing the water retention curve is chosen to reproduce the measured data:

$$S_{r,w} = S_{r,res} + CSW3\frac{(S_{r,field} - S_{r,res})}{CSW3 + (CSW1.s)^{CSW2}} \qquad (4.1)$$

where $S_{r,field}$ is the maximum saturation in the soil and
$S_{r,res}$ is the residual saturation for a very high value of suction.

The water relative permeability is determined by:

$$k_{r,w} = \frac{\left(S_{r,w} - S_{r,res}\right)^{CKW}}{\left(S_{r,field} - S_{r,res}\right)^{CKW}} \text{ if } S_{r,w} \geq S_{r,res}$$
$$k_{r,w} = k_{r,w,\min} \qquad \text{if } S_{r,w} < S_{r,res} \qquad (4.2)$$

The gas relative permeability is modelled by:

$$k_{r,g} = (1 - S_e)^{CKA1}.\left(1 - S_e^{CKA2}\right) \qquad (4.3)$$

with S_e the effective saturation.

The water retention curve and the permeability are found to have an important influence on the water intake volume and the final saturation degree. The soil conductivity is a function of the saturation degree.

4.2 Parameters related to the mechanical model

Two series of suction controlled oedometer tests have been realised to get the mechanical parameters. First one includes some tests with wetting-drying cycles under different constant vertical pressures. Another series of tests have been realised following several loading-unloading cycles under different constant suctions. By the way, the suction yield parameter s_0 is obtained by the water retention curve.

4.3 Comparison between simulation and experimental results

The figure 4.2 shows the water intake evolution with the time. A very good result is obtained: the experimental and numerical curves are almost the same.

The figure 4.3 shows the comparison between experimental and numerical result of the swelling pressure at the point with co-ordinates r=7.5 cm and z=1.25 cm during the experience. The agreement is good at the beginning, but decreases at the end of

experience. In fact, the model didn't take into account some variations of certain parameters for this simulation, like that κ_s varies with the net stress, κ depends on the suction, etc.

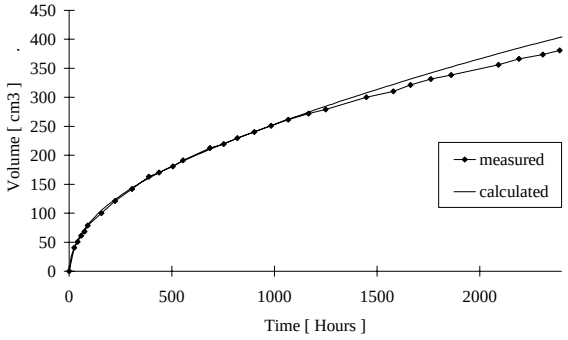

Fig. 4.2 Water intake evolution

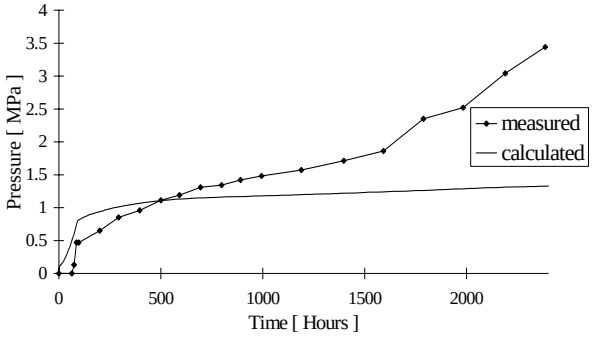

Fig. 4.3 Swelling pressure evolution

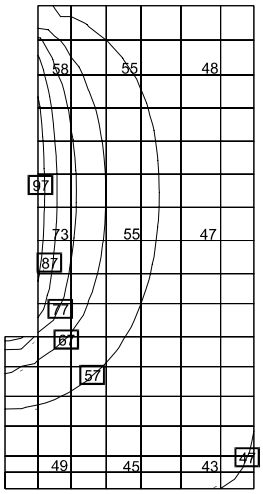

Fig.4.4 Temperature field at the end of experience

The calculated temperatures and water contents at the end of experience are given in the figure 4.4 and 4.5 respectively. The corresponding experimental measurements at some points are also presented on the same figure. The calculated temperatures are a little higher than the experimental ones. The numerical water content seems to be slightly lower than the experimental one at the analysed points. But they are close to the experimental ones near the heater. The generation of water vapour near the heater is a crucial phenomenon to be taken here in account. The vapour flow depends deeply on the temperature.

All the results appear to be very sensitive to the retention curve, the relative and intrinsic permeability.

A last remark could be that the soil mechanics has not a high influence on the water flow. Oppositely, the water flow has a deep influence on the mechanical behaviour.

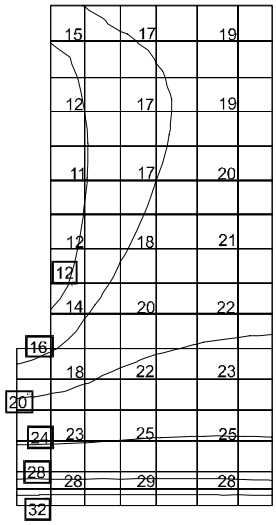

Fig.4.5 Water content at the end of experience

5. CONCLUSION

A complete theory on the thermo-hydro-mechanical coupling model in the unsaturated soil is provided in this paper. A validation test is performed to show the capabilities of the model to simulate the relevant phenomenon in a nuclear energy storage framework. The comparison between simulation results and experimental ones are analysed.

ACKNOWLEDGEMENTS

The authors thank the Europe Community for the support through the research project *Catsius clay* project. The support from FNRS is also greatly acknowledges.

REFERENCES

Alonso, E.E. & Gens, A. & Josa, A.A. 1990. A constitutive model for partly saturated soil. *Géotechnique*. 40, n°3: 405-430.

Edlefsen, N. E. & Anderson, A.B.C. 1943. Thermodynamics of soils moisture. *Hilgardia* 15, No. 2, 31-298.

Fredlund, D.G. & Morgenstern, N.R. 1977. Stress state variables for unsaturated soils. *J. Geotech. Eng. Div. A.S.C.E.* 103 GT5. 447-466.

Philip, J.R. & de Vries, D.A. 1957. Moisture movement in porous materials under temperature gradients. *Trans. Am. Geophys. Un.* 38, 222-232.